Buckling of Imperfect Elastic Shells using the Asymptotic Numerical Method

Sébastien Baguet, Bruno Cochelin

ECCM-2001
European Conference on
Computational Mechanics
June 26-29, 2001
Cracow, Poland

Buckling of Imperfect Elastic Shells using the Asymptotic Numerical Method

S. Baguet and B. Cochelin

Laboratoire de Mécanique et d'Acoustique CNRS UPR 7051
Ecole Supérieure de Mécanique de Marseille, IMT Technopôle de Château Gombert
13451 Marseille Cedex 20 - France
e–mail: baguet@mn.esm2.imt-mrs.fr, cochelin@mn.esm2.imt-mrs.fr

Key words: Instabilities, Fold Line, Augmented System, Asymptotic Numerical Method, Nonlinear Shells, Finite Elements

Abstract. *This paper is concerned with stability behaviour and imperfection sensitivity of elastic shells. The aim is to determine the reduction of the critical buckling load as a function of the imperfection amplitude. For this purpose, the direct calculation of the so-called fold line connecting all the limit points of the equilibrium branches of the imperfect structures is performed. An augmented system demanding the criticality of the equilibrium is used. In order to solve the augmented system, the Asymptotic Numerical Method is used as an alternative to Newton-like incremental-iterative procedures. It results in a very robust and efficient path-following algorithm that takes the singularity of the tangent stiffness matrix into account. Two specific types of imperfections are detailed and several numerical examples are discussed.*

1 Introduction

The development of new materials and the wide use of optimization techniques over the past decades have conducted to very light but robust structures. However, for such slender structures, structural stability has become a question of prime interest.

This stability analysis is all the more complex that such structures are often very sensitive to imperfections. A small defect can significantly reduce the critical buckling load, causing the collapse of the structure for a far smaller value than in the case of a perfect structure. The manufacturing of the structure, unusual loadings, shocks or corrosion for example can cause such defects. This imperfection sensitivity analysis will be discussed here in the case of thickness or geometrical shape imperfections.

This analysis deals with two specific problems. On one hand, it concerns the evaluation of the equilibrium branch of the structure and the precise detection of the associated singular points. This is a common post-buckling problem. In the case of quasi-static linear elasticity, it can be represented by the following one-parameter system

$$\boldsymbol{F}(\boldsymbol{u},\lambda) = \boldsymbol{f}(\boldsymbol{u}) - \boldsymbol{p}(\lambda) = 0 \tag{1}$$

where the external loading $\boldsymbol{p}$ is assumed linearly proportional and the internal forces $\boldsymbol{f}$ depend only on the displacement $\boldsymbol{u}$. This nonlinear system is usually solved using an incremental-iterative Newton-like procedure.

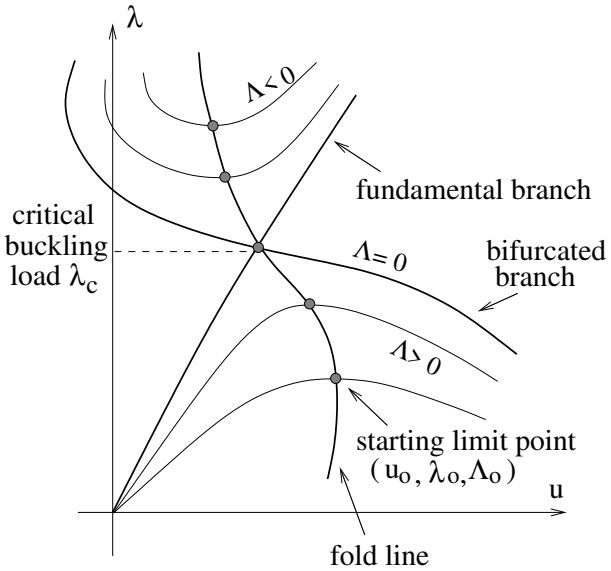

Figure 1: Fold line connecting the limit points and equilibrium branches for the perfect and imperfect structure

On the other hand, our analysis is concerned with the imperfection sensitivity of the structure. The aim is to study the variation of the critical buckling load when the structure is subjected to a variable imperfection. A simple way for carrying this analysis consists in introducing an imperfection in the structure and in solving problem (1) for the modified structure. Once this

calculation has been performed for different values of the imperfection, the grid of equilibrium branches and their associated limit points can be represented as in Figure 1. The fold line connecting the different limit points can then be drawn.

Even if this type of analysis is very simple to implement, it has major drawbacks. Indeed, this succession of re-analyses is very costly since it requires a full computation on the structure for each requested limit point. In order to reduce the computational time it is more advisable to to isolate a starting limit point for a given value of the imperfection and then to directly follow the branch of limit point. To this end, the imperfection amplitude Λ must become an additional parameter in the governing equations of the structure

$$\boldsymbol{F}(\boldsymbol{u}, \lambda, \Lambda) = \boldsymbol{f}(\boldsymbol{u}, \Lambda) - p(\lambda) = 0 \tag{2}$$

Doing so, the classical 1D "loading-displacement" solution sets become 2D " loading-imperfection-displacement" solution sets. On these surfaces, we are only interested in the critical points that give the variation of the critical load with respect to the imperfection amplitude. In order to directly obtain the branches of critical (limit) points, a constraint equation characterizing the limit points is appended to the equilibrium equation. The two-parameter nonlinear system (2) is then transformed in a so-called 'augmented' system which reads

$$\boldsymbol{R}\left(\boldsymbol{u}, \lambda, \Lambda\right) = \left(\begin{array}{c} \boldsymbol{F}\left(\boldsymbol{u}, \lambda, \Lambda\right) \\ \boldsymbol{G}\left(\boldsymbol{u}, \Lambda\right) \end{array} \right) = 0 \tag{3}$$

This augmented system has already been addressed by Jepson and Spence [1] , Wagner and Wriggers [2], and Eriksson [3] using incremental-iterative strategies. The originality of this work lies in the use of the Asymptotic Numerical Method (A.N.M.) in order to numerically solve this problem.

2 Fold line following

This section is devoted to the direct computation of the fold line connecting all the limit points of $\boldsymbol{F}$ when the imperfection varies. For this purpose, we assume that a starting limit point has already been detected. As mentioned in the introduction, this preliminary work consists in computing an equilibrium branch for a given value of the imperfection and in precisely calculating the limit state corresponding to the critical buckling load. This stage will not be discussed here (see [4] and [5]).

2.1 Augmented problem

Many alternatives concerning thconstraint equation $\boldsymbol{G}\left(\boldsymbol{u}, \Lambda\right)$=0 have been proposed in the literature. From a numerical point of view, the most efficient of these alternatives is due to Keener and Keller [6]. It has been subsequently used by Moore and Spence [7], Jepson and Spence [1], and numerically investigated by Wriggers and Simo [8] and Eriksson et al. [9] among others.

It is based on the appearance of a null eigenvalue for the tangent operator $\boldsymbol{K}_T = \boldsymbol{F}_{,\boldsymbol{u}}$ at simple critical states. This vector criterium leads to the following augmented system

$$\boldsymbol{R}\left(\boldsymbol{u},\boldsymbol{\varphi},\Lambda,\lambda\right) = \left(\begin{array}{c} \boldsymbol{F}\left(\boldsymbol{u},\Lambda,\lambda\right) \\ \boldsymbol{F}_{,\boldsymbol{u}}\left(\boldsymbol{u},\Lambda,\lambda\right)\cdot\boldsymbol{\varphi} \\ \|\boldsymbol{\varphi}\|-1 \end{array} \right) = \left(\begin{array}{c} \boldsymbol{f}\left(\boldsymbol{u},\Lambda\right)-\lambda\boldsymbol{F}_e \\ \boldsymbol{f}_{,\boldsymbol{u}}\left(\boldsymbol{u},\Lambda\right)\cdot\boldsymbol{\varphi} \\ \|\boldsymbol{\varphi}\|-1 \end{array} \right) = 0 \tag{4}$$

where $\boldsymbol{\varphi}$ is the null eigenvector associated with the null eigenvalue. The last normalization condition ensures its uniqueness.

2.2 Asymptotic Numerical Method (A.N.M.)

The previous two-parameter nonlinear augmented system (4) is solved using the Asymptotic Numerical Method (A.N.M.). This method is inspired by the perturbation techniques developed by Thompson and Walker [10] and used by Noor et al. [11] for designing "reduced bases" algorithms. These perturbation techniques have been revisited by Cochelin, Damil and Potier-Ferry [12, 13, 14] who coupled them with the finite element method to produce a very efficient algorithm.

2.2.1 Power series expansions

Assuming that a starting limit point $(\boldsymbol{u}_0,\boldsymbol{\varphi}_0,\lambda_0,\Lambda_0)$ is known, the basic idea of the A.N.M. consists in seeking the solution branch $(\boldsymbol{u},\boldsymbol{\varphi},\lambda,\Lambda)$ in a truncated power series form with respect to a well chosen path parameter "a"

$$\begin{aligned} \boldsymbol{u}(a) &= \boldsymbol{u}_0 + a\,\boldsymbol{u}_1 + a^2\,\boldsymbol{u}_2 + \ldots + a^n\,\boldsymbol{u}_n \\ \boldsymbol{\varphi}(a) &= \boldsymbol{\varphi}_0 + a\,\boldsymbol{\varphi}_1 + a^2\,\boldsymbol{\varphi}_2 + \ldots + a^n\,\boldsymbol{\varphi}_n \\ \lambda(a) &= \lambda_0 + a\,\lambda_1 + a^2\,\lambda_2 + \ldots + a^n\,\lambda_n \\ \Lambda(a) &= \Lambda_0 + a\,\Lambda_1 + a^2\,\Lambda_2 + \ldots + a^n\,\Lambda_n \end{aligned} \tag{5}$$

Because of the extra variable a, an additional equation is needed. This equation can be inspired by the well-known arc-length continuation method. In that case, a is defined as follows

$$a = \langle \boldsymbol{u}-\boldsymbol{u}_0,\boldsymbol{u}_1\rangle + (\lambda-\lambda_0)\lambda_1 + (\Lambda-\Lambda_0)\Lambda_1 \tag{6}$$

Introducing the developments (5) into the nonlinear system (4) and the scaling equation (6) and identifying the power-like terms leads to a succession of well-posed linear problems. The problem at order 1 reads

$$\left[\begin{array}{cccc} \boldsymbol{f}_{,\boldsymbol{u}} & 0 & \boldsymbol{f}_{,\Lambda} & -\boldsymbol{F}_e \\ \boldsymbol{f}_{,\boldsymbol{u}\boldsymbol{u}}\cdot\boldsymbol{\varphi}_0 & \boldsymbol{f}_{,\boldsymbol{u}} & \boldsymbol{f}_{,\boldsymbol{u}\Lambda}\cdot\boldsymbol{\varphi}_0 & 0 \\ 0 & \boldsymbol{\varphi}_0^t & 0 & 0 \\ \boldsymbol{u}_1^t & 0 & \Lambda_1 & \lambda_1 \end{array} \right] \left\{ \begin{array}{c} \boldsymbol{u}_1 \\ \boldsymbol{\varphi}_1 \\ \Lambda_1 \\ \lambda_1 \end{array} \right\} = 0 \tag{7}$$

This linear system gives the tangent direction $(\boldsymbol{u}_1,\boldsymbol{\varphi}_1,\Lambda_1,\lambda_1)$. It is exactly the same system as for the predictor step in the incremental-iterative Newton-Raphson algorithm. It also exhibits

the augmented tangent operator which will be the same for all other orders. The problem at order p ($p \geq 2$) reads

$$\begin{bmatrix} \boldsymbol{f}_{,\boldsymbol{u}} & 0 & \boldsymbol{f}_{,\Lambda} & -\boldsymbol{F}_e \\ \boldsymbol{f}_{,\boldsymbol{u}\boldsymbol{u}} \cdot \boldsymbol{\varphi}_0 & \boldsymbol{f}_{,\boldsymbol{u}} & \boldsymbol{f}_{,\boldsymbol{u}\Lambda} \cdot \boldsymbol{\varphi}_0 & 0 \\ 0 & \boldsymbol{\varphi}_0^t & 0 & 0 \\ \boldsymbol{u}_1^t & 0 & \Lambda_1 & \lambda_1 \end{bmatrix} \begin{Bmatrix} \boldsymbol{u}_p \\ \boldsymbol{\varphi}_p \\ \Lambda_p \\ \lambda_p \end{Bmatrix} = \begin{Bmatrix} r.h.s. \\ r.h.s. \\ r.h.s. \\ r.h.s. \end{Bmatrix} \tag{8}$$

The difference with order 1 lies in the r.h.s. vector which is not null anymore. This r.h.s depends on the solution at previous orders. Thus, the succession of linear problems can be solved in a recursive way with the same tangent operator for each order.

The next step of the A.N.M. lies in the use of a finite element method in order to transform the previous continuous problem into a discretized one. This will allow the succession of linear problems to be solved efficiently.

2.2.2 Finite elements discretization

After FEM discretization, the displacement problem at order p ($p \geq 2$) reads

$$\begin{bmatrix} \boldsymbol{K}_T & 0 & \boldsymbol{F}_1 & -\boldsymbol{F}_e \\ \boldsymbol{K}_{\boldsymbol{\varphi}} & \boldsymbol{K}_T & \boldsymbol{F}_2 & 0 \\ 0 & \boldsymbol{\varphi}_0^t & 0 & 0 \\ \boldsymbol{u}_1^t & 0 & \Lambda_1 & \lambda_1 \end{bmatrix} \begin{bmatrix} \boldsymbol{u}_p \\ \boldsymbol{\varphi}_p \\ \Lambda_p \\ \lambda_p \end{bmatrix} = \begin{bmatrix} \boldsymbol{F}_p^{nl} \\ \boldsymbol{G}_p^{nl} \\ h_p^{nl} \\ 0 \end{bmatrix} \quad \begin{matrix} \textit{(N eq.)} \\ \textit{(N eq.)} \\ \textit{(1 eq.)} \\ \textit{(1 eq.)} \end{matrix} \tag{9}$$

$\boldsymbol{K}_T$ is the classical tangent stiffness matrix, calculated at the starting point. Its expression is given by

$$\boldsymbol{K}_T(\boldsymbol{u}_0) = f_{,\boldsymbol{u}}(\boldsymbol{u}_0) = \int_\Omega \left(\boldsymbol{B}^t(\boldsymbol{u}_0)\, \boldsymbol{D}\, \boldsymbol{B}_{nl}(\boldsymbol{u}_0) + \boldsymbol{G}^t\, \hat{\boldsymbol{S}}_0\, \boldsymbol{G} \right) d\Omega \tag{10}$$

with $\boldsymbol{B}(\boldsymbol{u})$=$\boldsymbol{B}_l$+$\boldsymbol{B}_{nl}(\boldsymbol{u})$. Here $\boldsymbol{B}_l$ and $\boldsymbol{B}_{nl}(\boldsymbol{u})$ are the linear and nonlinear parts of the Green-Lagrange strain [15]. The matrix $\hat{\boldsymbol{S}}_0$ contains the components of the second Piola Kirchhoff stress $\boldsymbol{S}_0$ associated with $\boldsymbol{u}_0$ and $\boldsymbol{D}$ is the classical matrix which contains the elasticity constants. Using the same notations $\boldsymbol{K}_{\boldsymbol{\varphi}}$ reads

$$\boldsymbol{K}_{\boldsymbol{\varphi}}(\boldsymbol{u}_0, \boldsymbol{\varphi}_0) = f_{,\boldsymbol{u}\boldsymbol{u}} \cdot \boldsymbol{\varphi}_0 = \int_\Omega \left(\boldsymbol{B}^t(\boldsymbol{u}_0)\, \boldsymbol{D}\, \boldsymbol{B}_{nl}(\boldsymbol{\varphi}_0) + \boldsymbol{B}_{nl}^t(\boldsymbol{\varphi}_0)\, \boldsymbol{D}\, \boldsymbol{B}(\boldsymbol{u}_0) + \boldsymbol{G}^t\, \hat{\boldsymbol{\Psi}}_0\, \boldsymbol{G} \right) d\Omega \tag{11}$$

where $\hat{\boldsymbol{\Psi}}_0$ contains the components of the second Piola Kirchhoff stress $\boldsymbol{\Psi}_0$ associated with $\boldsymbol{\varphi}_0$.

The two matrices $\boldsymbol{K}_T$ and $\boldsymbol{K}_{\boldsymbol{\varphi}}$ are the same whatever the type of imperfection is. In the tangent operator, only the two vectors $\boldsymbol{F}_1$ and $\boldsymbol{F}_2$ depend on the imperfection. Indeed, they are the derivatives of $\boldsymbol{f}$ with respect to the imperfection Λ

$$\boldsymbol{F}_1(\boldsymbol{u}_0) = \boldsymbol{f}_{,\Lambda}(\boldsymbol{u}_0) \qquad \boldsymbol{F}_2(\boldsymbol{u}_0, \boldsymbol{\varphi}_0) = \boldsymbol{f}_{,\boldsymbol{u}\Lambda}(\boldsymbol{u}_0) \cdot \boldsymbol{\varphi}_0 \tag{12}$$

The r.h.s. terms $\boldsymbol{F}_p^{nl}$ and $\boldsymbol{G}_p^{nl}$ also depend on the type of imperfection. Their expressions will be detailed in section 3 in the case of a geometrical shape imperfection and in the case of a thickness imperfection.

These considerations are of prime interest. Indeed, they allow the implementation of a fairly general algorithm for solving (9). The only thing to keep in mind is to switch to the correct expressions of the vectors $\boldsymbol{F}_1$, $\boldsymbol{F}_2$, $\boldsymbol{F}_p^{nl}$ and $\boldsymbol{G}_p^{nl}$ according to the type of imperfection.

2.2.3 Deflated block elimination

In practice, a deflated block elimination is used to solve the extended system (9) in order to consider only subsystems of size N involving the $\boldsymbol{K}_T$ matrix. Such a block-elimination scheme can be found in Wriggers and Simo [8]. Its main interest relies on the fact that only the classical $\boldsymbol{K}_T$ matrix needs to be decomposed, thus saving a large amount of calculation time.

Besides this particular procedure, another numerical difficulty must be pointed out. Since all the solution points of $\boldsymbol{R}$ are singular ones of $\boldsymbol{F}$, the $\boldsymbol{K}_T$ matrix is singular all along the fold line connecting the computed solution points. That means that the classical matrix decomposition techniques cannot be used. A special procedure, based on Lagrange multipliers, is introduced to bypass this problem.

For a detailed description of the adaptation of the block-elimination and Lagrange multipliers procedures to the system (9), the interested reader is referred to [5].

2.2.4 Continuation method

Because of the limited radius of convergence of the series, only a fraction of the solution curve is obtained. The accuracy of the solution often deteriorates very quickly when the radius of convergence is reached. Cochelin has proposed a residual criterium that gives the length of a step [16]. For series truncated at order n, the maximal value of the path parameter a for which the solution satisfies a requested accuracy ε is given by

$$a_M = \left(\frac{\varepsilon}{\| \boldsymbol{F}_{n+1}^{nl} \|} \right)^{\frac{1}{n+1}} \tag{13}$$

Using this formula, the step length is set after all the coefficients of the series have been computed. By this way, the step length is guaranteed to be optimal.

Once the step has been stopped, the starting point is updated and the global procedure is restarted. Thus, the solution curve is described in a step by step way, as it would be with the classical continuation algorithms. The strong point of this procedure is its robustness. Furthermore, it is completely automatic from the user's point of view. The only parameters that need to be chosen are the order n of the series and the accuracy ε. Setting n equal to 20 or 30 and $\varepsilon = 10^{-6}$ is often a good compromise. Practice has demonstrated that computing higher orders to extend the step length is not worth the required extra calculation time.

3 Two specific types of imperfections

3.1 Geometrical shape imperfection

A variable geometrical shape imperfection $\boldsymbol{u}^\star$ is introduced within the structure. In order to get a scalar parameter, this imperfection is rewritten in the form

$$\boldsymbol{u}^\star = \eta\, \boldsymbol{u}_0^\star \tag{14}$$

where $\boldsymbol{u}_0^\star$ is a fixed vector that gives the shape of the imperfection and η is its amplitude. Here the amplitude η stands for the parameter Λ of section 2. The resulting governing equation (2) of the imperfect structure is

$$\boldsymbol{F}(\boldsymbol{u},\eta,\lambda) = \left\{ \begin{array}{l} \displaystyle\int_\Omega \boldsymbol{B}^t(\boldsymbol{u})\,\boldsymbol{S} + \eta\,\boldsymbol{B}_{nl}^t(\boldsymbol{u}_0^\star)\,\boldsymbol{S}\; d\Omega - \lambda \boldsymbol{F}_e = 0 \\ \quad \boldsymbol{S} = \boldsymbol{D}\;\left(\boldsymbol{B}_l + \frac{1}{2}\boldsymbol{B}_{nl}(\boldsymbol{u}) + \eta\,\boldsymbol{B}_{nl}(\boldsymbol{u}_0^\star)\right)\,\boldsymbol{u} \end{array} \right. \tag{15}$$

The needed calculations to obtain $\boldsymbol{F}_1$, $\boldsymbol{F}_2$, $\boldsymbol{F}_p^{nl}$ and $\boldsymbol{G}_p^{nl}$ are detailed in [5]. They will not be reproduced here. It finally leads to

$$\begin{aligned} \boldsymbol{F}_1 &= \int_\Omega \left(\tilde{\boldsymbol{B}}_0^t\,\boldsymbol{D}\,\boldsymbol{B}_{nl}(\boldsymbol{u}_0) + \boldsymbol{G}^t\,\hat{\boldsymbol{S}}_0\,\boldsymbol{G}\right)\,\boldsymbol{u}_0^\star\; d\Omega \\ \boldsymbol{F}_2 &= \int_\Omega \left(\tilde{\boldsymbol{B}}_0^t\,\boldsymbol{D}\,\boldsymbol{B}_{nl}(\boldsymbol{\varphi}_0) + \boldsymbol{B}_{nl}(\boldsymbol{\varphi}_0)\,\boldsymbol{D}\,\boldsymbol{B}_{nl}(\boldsymbol{u}_0) + \boldsymbol{G}^t\,\hat{\boldsymbol{\Psi}}_0\,\boldsymbol{G}\right)\,\boldsymbol{u}_0^\star\; d\Omega \\ \boldsymbol{F}_p^{nl} &= -\int_\Omega \tilde{\boldsymbol{B}}_0^t\,\boldsymbol{S}_p^{nl} + \sum_{r=1}^{p-1} \boldsymbol{B}_{nl}^t(\boldsymbol{u}_r + \eta_r \boldsymbol{u}_0^\star)\,\boldsymbol{S}_{p-r}\; d\Omega \\ \boldsymbol{G}_p^{nl} &= -\int_\Omega \tilde{\boldsymbol{B}}_0^t\,\boldsymbol{\Psi}_p^{nl} + \boldsymbol{B}_{nl}^t(\boldsymbol{\varphi}_0)\,\boldsymbol{S}_p^{nl} + \sum_{r=1}^{p-1} \boldsymbol{B}_{nl}^t(\boldsymbol{\varphi}_r)\,\boldsymbol{S}_{p-r} + \sum_{r=1}^{p-1} \boldsymbol{B}_{nl}^t(\boldsymbol{u}_r + \eta_r \boldsymbol{u}_0^\star)\,\boldsymbol{\Psi}_{p-r}\; d\Omega \end{aligned} \tag{16}$$

where $\tilde{\boldsymbol{B}}_0$ stands for $\boldsymbol{B}(\boldsymbol{u}_0 + \eta_0 \boldsymbol{u}_0^\star)$ and the pre-stress terms $\boldsymbol{S}_p^{nl}$ and $\boldsymbol{\Psi}_p^{nl}$ read

$$\begin{aligned} \boldsymbol{S}_p^{nl} &= \frac{1}{2}\,\boldsymbol{D} \sum_{r=1}^{p-1} \boldsymbol{B}_{nl}(\boldsymbol{u}_r)\,\boldsymbol{u}_{p-r} + \boldsymbol{D} \sum_{r=1}^{p-1} \eta_{p-r} \boldsymbol{B}_{nl}(\boldsymbol{u}_r)\,\boldsymbol{u}_0^\star \\ \boldsymbol{\Psi}_p^{nl} &= \boldsymbol{D} \sum_{r=1}^{p-1} \boldsymbol{B}_{nl}(\boldsymbol{\varphi}_r)\,\boldsymbol{u}_{p-r} + \boldsymbol{D} \sum_{r=1}^{p-1} \eta_{p-r} \boldsymbol{B}_{nl}(\boldsymbol{\varphi}_r)\,\boldsymbol{u}_0^\star \end{aligned} \tag{17}$$

$\boldsymbol{S}_k$ and $\boldsymbol{\Psi}_k$ are the second Piola Kirchhoff stresses associated with $\boldsymbol{u}_k$ and $\boldsymbol{\varphi}_k$.

3.2 Thickness imperfection

In this section, the additional parameter Λ of section 2 is the thickness h of the structure. In order to simplify the study, we focus on shell elements which are analytically integrated through the

thickness, and where the thickness explicitly appears only in the matrix of elasticity constants $\boldsymbol{D}$. For this class of shell elements, the elasticity matrix $\boldsymbol{D}$ can be decomposed into a membrane part and into a bending part, which are respectively linear and cubic with respect to h.

$$\boldsymbol{D}(h) = \boldsymbol{D}^1\, h + \boldsymbol{D}^3\, h^3 \tag{18}$$

The governing equation (2) becomes

$$\boldsymbol{F}(\boldsymbol{u}, h, \lambda) = \left\{ \begin{array}{l} \displaystyle\int_\Omega \boldsymbol{B}^t(\boldsymbol{u})\, \boldsymbol{S}\; d\Omega - \lambda \boldsymbol{F}_e = 0 \\ \boldsymbol{S} = \boldsymbol{D}(h)\;\; \left(\boldsymbol{B}_l + \frac{1}{2}\boldsymbol{B}_{nl}(\boldsymbol{u})\right)\, \boldsymbol{u} \end{array} \right. \tag{19}$$

Introducing the series expansion of h into $\boldsymbol{D}$ and replacing this expression into the augmented system (4) leads to

$$\begin{aligned} \boldsymbol{F}_1 &= \int_\Omega \boldsymbol{B}^t(\boldsymbol{u}_0)\, \tilde{\boldsymbol{D}}\, (\boldsymbol{B}_l + \tfrac{1}{2}\boldsymbol{B}_{nl}(\boldsymbol{u}_0))\, \boldsymbol{u}_0\; d\Omega \\ \boldsymbol{F}_2 &= \int_\Omega \boldsymbol{B}^t(\boldsymbol{u}_0)\, \tilde{\boldsymbol{D}}\, \boldsymbol{B}(\boldsymbol{u}_0)\, \boldsymbol{\varphi}_0 + \boldsymbol{B}_{nl}^t(\boldsymbol{\varphi}_0)\, \tilde{\boldsymbol{D}}\, (\boldsymbol{B}_l + \tfrac{1}{2}\boldsymbol{B}_{nl}(\boldsymbol{u}_0))\, \boldsymbol{u}_0\; d\Omega \end{aligned} \tag{20}$$

with

$$\tilde{\boldsymbol{D}} = \boldsymbol{D}^1 + 3h_0^2\, \boldsymbol{D}^3 \tag{21}$$

The expressions of $\boldsymbol{S}_p^{nl}$ and $\boldsymbol{\Psi}_p^{nl}$ are more complex and will not be given here. They will be fully detailed in a forthcoming paper.

4 Numerical examples

4.1 Cylindrical panel with shape imperfection

This first example is concerned with a cylindrical panel submitted to a concentrated load at its top. The geometrical and material properties and the boundary conditions of the panel are defined in Figure 2a. This is a typical buckling example which involves limit points and snap-through phenomenon. The aim of this example is to analyze the sensitivity of the critical buckling load of the cylindrical panel to a geometrical shape imperfection. At first, the analysis was performed on one half of the perfect structure, i.e. without any shape imperfection, using symmetry conditions. For this purpose, a 20×10 mesh with 400 triangular DKT shell elements [17] and 1386 degrees of freedom was used. All the results were obtained with the Asymptotic Numerical Method. They are plotted in Figure 2b.

The fundamental equilibrium branch was obtained with only 12 A.N.M. continuation steps, i.e. with only 12 K_T tangent matrix decompositions. Two limit points and two bifurcation points were isolated. The bifurcated branch joining these two bifurcation points was also computed. This bifurcated branch and its corresponding bifurcation points disappear if only one quarter of

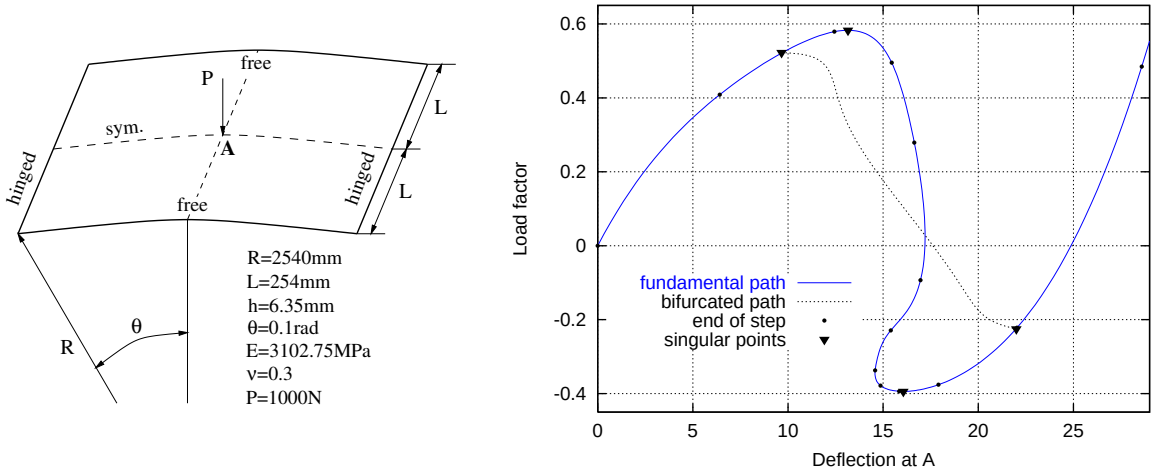

Figure 2: (a) Problem definition (b) Equilibrium curve of the perfect cylindrical panel

the panel is discretized. It can inferred from this remark that this bifurcation corresponds to a symmetry breaking.

Subsequently, the sensitivity analysis was conducted. Since we were only interested in the variation of the first limit point with respect to the imperfection amplitude, the bifurcation points were 'removed' by considering only one quarter of the panel, leading to a 10×10 mesh with 200 triangular DKT shell elements and 726 degrees of freedom. The first buckling eigenmode of the panel is shown in Figure 3. It was normalized by setting the greatest value of its displacement to 1 in order to provide the shape of the considered geometrical imperfection.

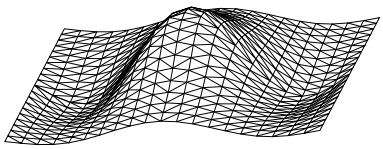

Figure 3: First buckling eigenmode of the perfect cylindrical panel

The procedure described in section 2 was then initiated to compute the fold line. This procedure is completely automatic. The user only has to provide the order n of the series expansions, the required accuracy ε for the solution, the number of steps and the initial imperfection amplitude η_0. A starting limit point is then isolated on the equilibrium branch of the structure including the initial imperfection and the fold-line following procedure is started from this limit point. This allows to choose any starting point for the fold curve and to follow it in either one direction (increasing imperfection amplitude) or the opposite one (decreasing imperfection amplitude).

For this example, the starting point was evaluated for an initial imperfection amplitude η_0=-3mm, i.e. -0.47 times the thickness of the panel. The curve shown in Figure 4 is a 3D representation of the resulting fold line connecting all the limit points when the imperfection varies. Its projections are more suited to our analysis. Two of them are represented in Figure 5. The first projection is located in the load-deflection plane. Three equilibrium branches are

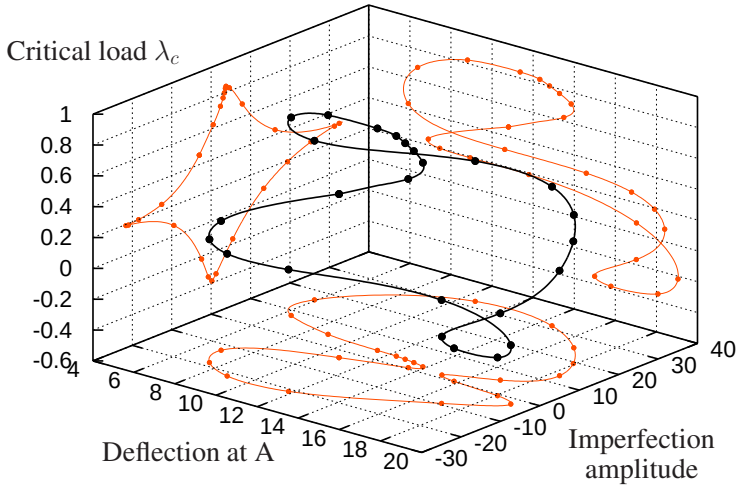

Figure 4: Cylindrical panel : 3D "load-deflection-imperfection" fold curve and its projections

plotted for different values of the imperfection as well as the projection of the fold line. The fold line intersects each equilibrium branch at its two limit points. The equilibrium branch of Figure 2b for the perfect panel is represented here again as a reference. The values of the load at its two limit points (maximum and minimum) can be also read on the right-hand-side Figure 5b which gives the critical buckling load reduction with respect to the imperfection. The top and bottom parts of this curve correspond respectively to the variation of the maximum and minimum limit point of the equilibrium curves. The curve shows that the two limit points get closer when the imperfection amplitude increases. For two extreme values $\eta/h\simeq$-3.5 and $\eta/h\simeq$5.3 of the imperfection, the limit points merge and exchange their role. Beyond these extreme values, there is no limit point anymore, i.e. no snap-through phenomenon anymore.

It can be noticed that the entire fold line was computed with only 25 continuation steps, i.e. only 25 tangent matrix decompositions.

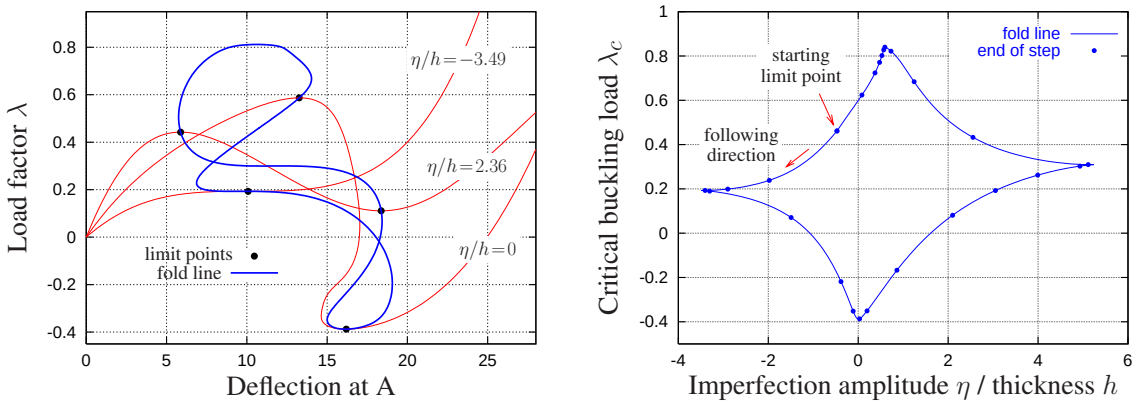

Figure 5: Cylindrical panel : (a) Fold line and equilibrium branches for various imperfection amplitudes with associated limit points (b) Critical buckling load reduction with respect to the imperfection

4.2 Cylindrical panel with thickness imperfection

The second example refers to the same cylindrical panel, with geometrical and material properties as defined in the previous section. The aim is now to analyze the sensitivity of the critical buckling load of the cylindrical panel to a thickness imperfection. This can be used to conduct a simplified corrosion analysis. For this purpose, the thickness h is chosen as the additional parameter Λ.

As before, after a starting limit point had been isolated, the fold line was followed using the Asymptotic Numerical Method. Its "load-deflection-thickness" 3D representation is plotted in Figure 6. This fold line was completely described with very few tangent matrix decompositions. Indeed, only 20 A.N.M. continuation steps with series at order 30 were computed. The projec-

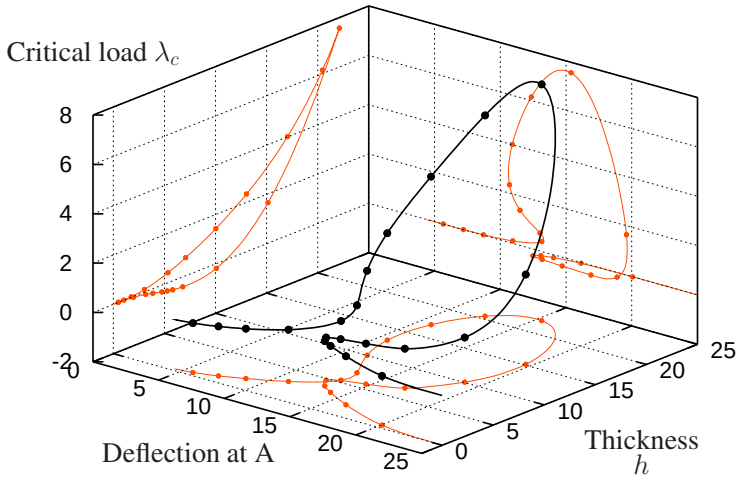

Figure 6: Cylindrical panel : 3D "load-deflection-thickness" fold curve and its projections

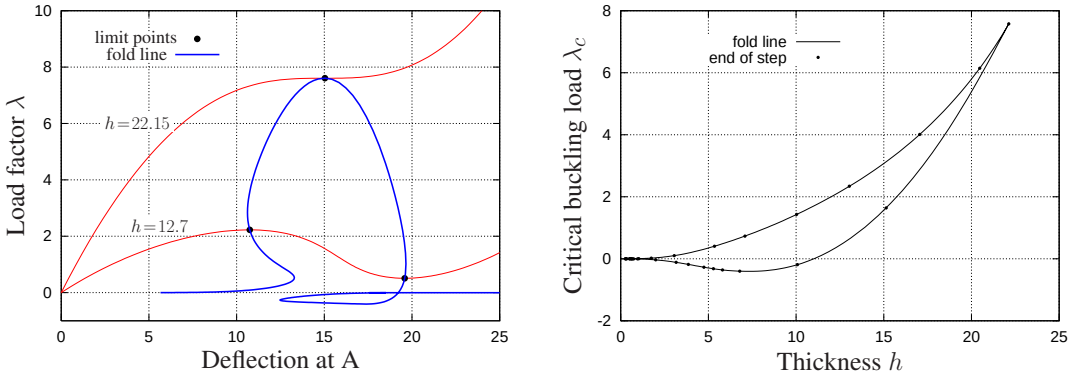

Figure 7: Cylindrical panel : (a) Fold line and equilibrium branches for various values of the thickness with associated limit points (b) Critical buckling load reduction with respect to the thickness

tions on the load-deflection plane and on the load-thickness plane are plotted in Figure 7. On the curve of Figure 7a, the fold line intersects the equilibrium branches at their two limit points, excepted for the extreme value $h \simeq 22.15$ of the thickness for which the two limit points merge into an inflection point. Beyond this value, there is no snap-through phenomenon anymore. This behaviour can also be observed on Figure 7b which shows the critical buckling load as a function of the panel thickness. For a given thickness, this curve gives the load corresponding to the maximum and the minimum limit points of the equilibrium branches of Figure 7a. The results obtained here are in very good agreement with those obtained by Eriksson et al. in [9].

4.3 Cylinder with geometrical shape imperfection under external pressure

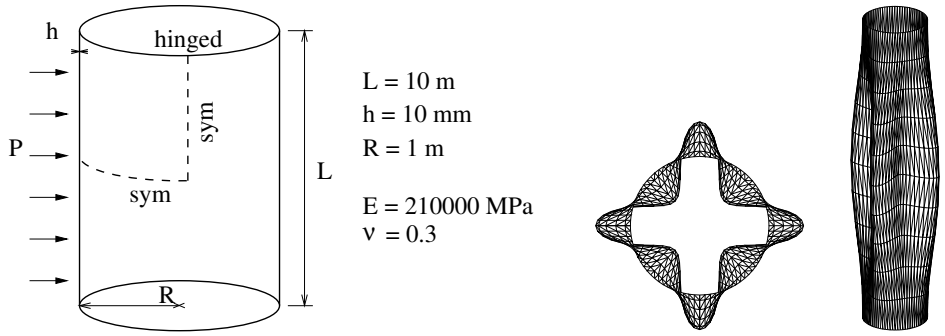

Figure 8: (a) Problem definition (b) First buckling eigenmode of the perfect cylinder (cross section and perspective)

The third example concerns the instability behaviour of a cylinder under external pressure, with geometrical and material properties as defined in Figure 8a. The aim is to investigate the sensitivity of the cylinder to a geometrical shape imperfection.

Using symmetry conditions and hinged boundary conditions, only one half of the cylinder in the longitudinal direction and a sector of 90° was discretized. A 32×5 mesh with 320 triangular DKT shell elements and 1188 degrees of freedom was used. The first buckling eigenmode shown in Figure 8b was used as the imperfection shape.

The fold-line following was initiated with an initial imperfection of one quarter of the thickness of the shell and performed in the two directions (increasing and decreasing imperfection) from this starting point. The resulting fold line and a few equilibrium branches for various values of the imperfection are plotted in Figure 9. An extreme value of the imperfection amplitude $\Lambda \simeq h/1.7$ was detected. Beyond this value, the equilibrium branches have no limit point anymore. Very few A.N.M. continuations steps were needed for this analyse. Indeed, the interesting part of the fold line (from Λ=0 up to $\Lambda \simeq h/1.7$) was obtained with only 6 continuation steps, i.e. 6 tangent matrix decompositions.

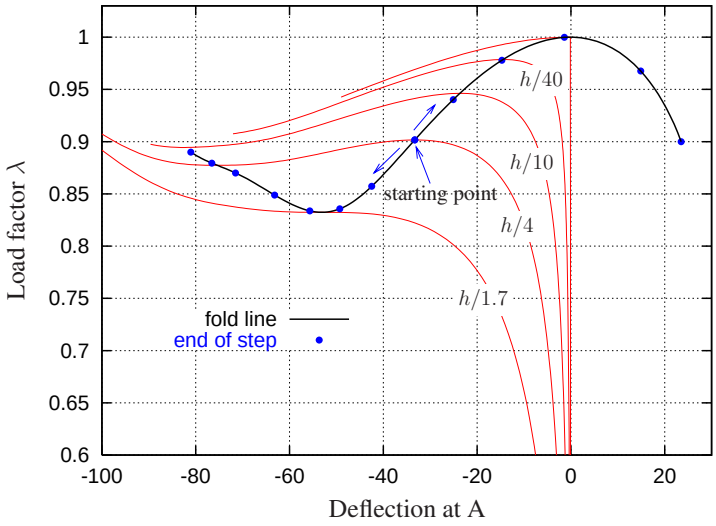

Figure 9: Fold line and equilibrium branches for imperfection amplitudes from 1/40 up to 1/1.7 times the thickness of the cylinder

4.4 Axially compressed cylinder with geometrical shape imperfection

The last example is concerned with a cylindrical shell under axial load with geometrical and material properties as in Figure 10a. It is certainly one of the most classical examples in shell stability analysis. It is also one of the most spectacular ones because the sensitivity to imperfections is very important. Here the considered imperfection is a geometrical one with a shape identical to the first eigenmode of the compressed cylinder, as represented in Figure 10b. Using symmetry conditions and hinged boundary conditions, only half of the length and a sector of 90° of the cylinder was discretized. A 32×5 mesh with 320 triangular DKT shell elements and 1188 degrees of freedom was used.

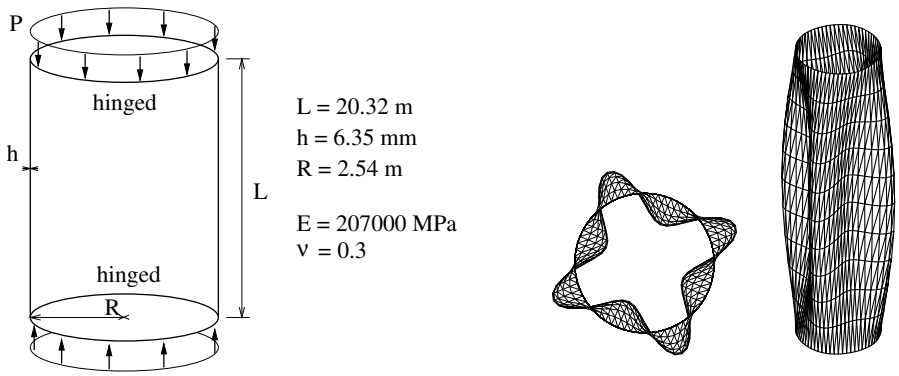

Figure 10: (a) Problem definition (b) First buckling eigenmode of the perfect cylinder (cross section and perspective)

The fold line connecting the limit point as well as five equilibrium branches for different values of the imperfection amplitude are plotted in Figure 11. No more limit points are observed beyond the value $\Lambda \simeq 19h$ of the imperfection amplitude. This value corresponds to a very seri-

ous critical load reduction. At this level, the critical buckling load is 80% smaller than for the perfect cylinder.

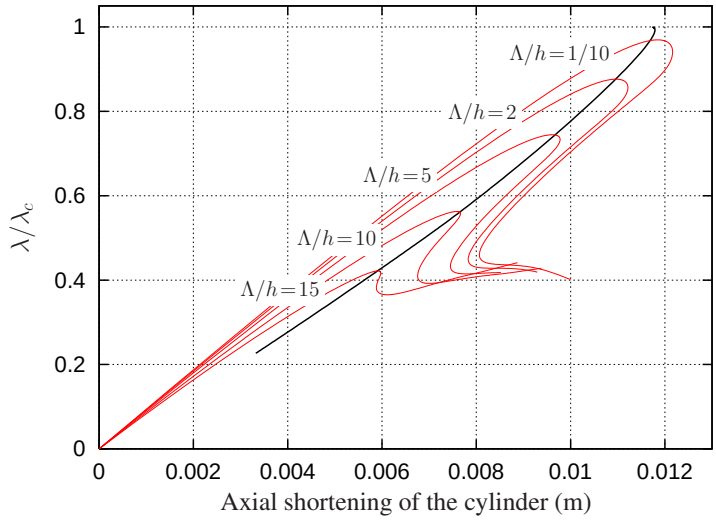

Figure 11: Fold line and equilibrium branches for imperfection amplitudes from 1/10 up to 15 times the thickness of the cylinder

5 Conclusions

This paper has described a general procedure for the stability analysis and the imperfection sensitivity analysis of elastic structures. The Asymptotic Numerical Method is used for the numerical treatment of the problem. The required calculation cost is significantly reduced as compared to the classical Newton-Raphson procedure. Moreover, this method is very robust and the associated continuation procedure is completely automatic from the user's point of view.

With the developed calculation tool, global as well as local imperfections can be treated, in the case of thickness or geometrical shape defects.

The future developments will concern the introduction of material nonlinearities. Also, a shell element which handles large rotations will be implemented.

References

[1] A.D. Jepson and A. Spence. Folds in solutions of two parameter systems and their calculation. part i. *SIAM J. Numer. Anal.*, **22**, 347–368, (1985).

[2] W. Wagner and P. Wriggers. Calculation of bifurcation points via fold curves. In W. Wagner and P. Wriggers, editors, *Nonlinear Computational Mechanics*, pages 69–84. Springer-Verlag, Berlin Heidelberg, (1991).

[3] A. Eriksson. Equilibrium subsets for multi-parametric structural analysis. *Comput. Methods Appl. Mech. Engrg.*, **140**, 305–327, (1997).

[4] E.H. Boutyour. Détection des bifurcations par des méthodes asymptotiques-numériques. In *Deuxième colloque national en calcul des structures*, volume 2, pages 687–692, Giens, France. May 1995.

[5] S. Baguet and B. Cochelin. Direct computation of paths of limit points using the asymptotic numerical method. In *IASS-IACM 2000, 4th International Colloquium on Computation of Shell & Spatial Structures*, Chania - Crete, Greece. June 5-7 2000.

[6] J.P. Keener and H.B. Keller. Perturbed bifurcation theory. *Arch. Rational Mech. Anal.*, **50**, 159–179, (1973).

[7] G. Moore and A. Spence. The calculation of turning points of nonlinear equations. *SIAM J. Numer. Anal.*, **17**, 567–576, (1980).

[8] P. Wriggers and J.C. Simo. A general procedure for the direct calculation of turning and bifurcation points. *Int. J. Numer. Meth. Eng.*, **30**, 155–176, (1990).

[9] A. Eriksson, C. Pacoste, and A. Zdunek. Numerical analysis of complex instability behaviour using incremental-iterative strategies. *Comput. Methods Appl. Mech. Engrg.*, **179**, 265–305, (1999).

[10] J.M.T. Thompson and A.C. Walker. The nonlinear perturbation analysis of discrete structural systems. *Int. J. Solids Structures*, **4**, 757–758, (1968).

[11] A.K. Noor and J.M. Peters. Reduced basis technique for nonlinear analysis of structures. *AIAA Journal - N4*, **18**, 455–462, (1980).

[12] N. Damil and M. Potier-Ferry. A new method to compute perturbed bifurcations: application to the buckling of imperfect elastic structures. *International Journal of Engineering Sciences - N9*, **28**, 943–957, (1990).

[13] B. Cochelin, N. Damil, and M. Potier-Ferry. The asymptotic-numerical-method: an efficient perturbation technique for nonlinear structural mechanics. *Revue Européenne des Eléments Finis*, **3**, 281–297, (1994).

[14] L. Azrar, B. Cochelin, N. Damil, and M. Potier-Ferry. An asymptotic numerical method to compute the post-buckling behavior of elastic plates and shells. *Int. J. Numer. Meth. Eng.*, **36**, 1251–1277, (1993).

[15] M.A. Crisfield. *Nonlinear Finite Element Analysis of Solids ans Structures, Vol.2*. John Wiley and Sons, 1st edition, (1997).

[16] B. Cochelin. A path following technique via an asymptotic numerical method. *Computers & Structures*, **29**, 1181–1192, (1994).

[17] J.L. Batoz and G.S. Dhatt. *Modélisation des structures par éléments finis*, volume 1,2,3. Eds Hermès, Paris, (1992).